Alternative dissipation mechanisms and the effect of the solvent in friction between polymer brushes on rough surfaces†

Sissi de Beer*[a] **and Martin H. Müser**[ab]

Received Xth XXXXXXXXXX 20XX, Accepted Xth XXXXXXXXX 20XX
First published on the web Xth XXXXXXXXXX 200X
DOI: 10.1039/b000000x

Surfaces covered with end-anchored polymers under good solvent conditions have excellent tribological properties. The friction between such surfaces is commonly attributed to steady-state interdigitation of the opposing polymer brushes. However, this conclusion tends to be based on idealized geometries neglecting surface roughness. Using molecular dynamics simulations, we find that there are qualitative differences between the friction of rough and flat polymer-brush surfaces. For rough surfaces the dissipation due to transient interdigitation and capillary- and shape-hysteresis is just as important or can even dominate over steady-state interdigitation. Having a mix of dissipation mechanisms that are all intertwined affects the observed friction force in linear-response as well as in the shear-thinning exponents and effective viscosity. Moreover, we find that the effect of the solvent viscosity is sublinear.

Introduction

To reduce friction and wear, moving parts need to be lubricated. An ideal lubricant stays in the contact during motion and at rest to prevent surfaces from touching and to diminish the subsequent damage. Plain water is usually an unsuitable lubricant, since it is easily squeezed out from zones with high local pressure gradients. Oils are better lubricants, because they increase their viscosity with increasing pressure and are therefore not squeezed out as quickly as water[1,2]. However, the best lubricants are found in biological contacts, e.g., in human joints. They manage to keep an aqueous liquid inside the contact over a wide range of pressures by the presence of hydrophilic polymers[3]. In the last decades there have been numerous attempts to port this principle to industrial[4–11] or even prosthetic[12] applications, in particular through grafting polymers to surfaces. Studying the lubricating properties of polymer brushes does not only benefit sliding solid interfaces but also affect colloidal motion, e.g., in the context of oil recovery and drug delivery[13,14].

When polymers in a good solvent are anchored by one end to solid surfaces, they will, depending on the grafting density, stand up to form soft brushes[15,16]. Upon pressing two of those polymer-bearing surfaces together, the brushes will keep the solvent from being squeezed out even when pressure gradients are large and thereby protect the surfaces.

Friction in sliding contacts of polymer brushes is commonly related to "combing" that results from the relative motion of overlapping or interdigitating polymers[17–20]. In particular molecular dynamics (MD) simulations, which allow one to quantify the amount of brush overlap in a straightforward fashion, reveal a strong correlation between interdigitation and friction[19–22]. Moreover, motivated from scaling arguments[23–25] a direct relation between friction and interdigitation has been derived, agreeing with both simulations[26,27] and experiments[28]. The scaling arguments do not depend on the polarity of the system, i.e., whether brushes and solvent are hydrophilic or hydrophobic. In fact, recent simulations reveal similar exponents of the friction velocity dependence for hydrophobic neutral and hydrophilic charged polyelectrolyte polymer brushes[29–31] unless the solvent hydrodynamics are fully screened[30]. The main difference seems to be that the polyelectrolyte brushes showed a smaller[32] or larger[30,31] prefactor in the friction. It is difficult to directly compare the effect of only the charges to experimental observations[33], because in experiments both the charges and the type of polymers will change. Interestingly, it was recently shown that for charged brushes the friction can be controlled through external electric fields[34].

Presently, the geometry considered in most experiments and simulations of brush friction is highly idealized, e.g., plane plates in simulations[19–21,26], crossed cylinders in surface forces apparatus (SFA) experiments[5,33,34], and sphere on a plate geometry in atomic force microscopy (AFM) experiments[7,10,11]. However, almost all surfaces have roughness on many lengthscales. As a consequence of their roughness, surfaces only touch at a minuscule fraction of the apparent

---

† Electronic Supplementary Information (ESI) available. See DOI: 10.1039/b000000x/

[a] *Jülich Supercomputing Centre, Institute for Advanced Simulation, FZ Jülich, Jülich, Germany; E-mail: s.de.beer@fz-juelich.de*
[b] *Dept. of Materials Science and Engineering, Universität des Saarlandes, Saarbrücken, Germany*

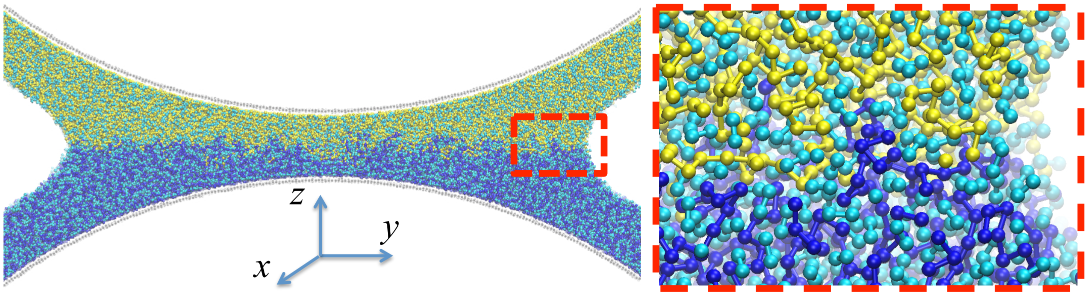

Fig. 1 Snapshot of our simulation cell. Two cylinders are set up in parallel. Polymers belonging to opposing brushes are colored differently (yellow and dark blue) but identical in physical properties. They are attracted to the one-phase solvent (light blue).

contact. Thus, in a sliding interface, contact stresses fluctuate significantly in space and time whenever two peaks from opposing surfaces bump into each other. These strong stress fluctuations are known to have a destructive effect on self-assembled monolayers (SAM)[35,36], which is particularly important in finding a proper lubricant for microelectromechanical systems (MEMS)[37]. Polymer brushes are less sensitive to wear, since the grafted polymers are in general more strongly attached to the surfaces and, in case they do come off[38], the surfaces can be healed by free flowing polymers in the solvent. It was recently shown in AFM experiments that surface roughness will decrease the adhesion between polymer-bearing surfaces[39]. Further, the friction due to asperity collisions of surface-adsorbed polymers is known to behave qualitatively different from the friction of flat interfaces[40].

Upon colliding brush-covered asperities alternative dissipation mechanisms can arise that are not captured in the idealized geometries described above. For example, visco-elastic deformation can lead to shape hysteresis, which is a major contribution to rubber friction[41,42]. In fact, recent simulations of non-centrally colliding star polymers indicate that losses due to shape hysteresis can dominate when polymers lack the time to interdigitate during contact[43]. On top of that, when the polymers do interdigitate, the slow relaxation of interdigitation will cause transient effects resulting in additional dissipation[44]. Also, during the collision the solvent will be expelled and re-absorbed into the brush causing viscous dissipation[45], as studied for head-on collisions[46]. Moreover, capillary formation and break-up due to the surface tension of the solvent can now also contribute to the dissipation[47]. For example, it is known from the friction of the human skin that a lot of sweat decreases the friction compared to dry sliding, but that a bit of sweat increases the friction due to the formation of small capillaries[48,49]. While all these effects can be studied in AFM and SFA experiments by separating the two surfaces in the direction normal to the interface, there is no general relation between the adhesive hysteresis under such normal motion and friction counteracting lateral motion[34,50–52].

Here we report MD simulations of the collision and the sliding of two parallel, curved, polymer-bearing surfaces. Upon moving in the parallel, transverse, and normal direction, we probe motion at a constant distance, off-center collisions and head-on collisions respectively. We find that, depending on the direction of motion a different mix of dissipation mechanisms can dominate the friction, even in linear response. Moreover, the effect of the solvent viscosity depends on the mix of dissipation mechanisms. This leads to the conclusion that polymer brush friction on rough surfaces is qualitatively different from the friction for polymer brushes on flat surfaces.

Model and Methods

In general, the polarity of polymer brush systems does not qualitatively alter the friction forces and (depending on the normal load[31]) only quantitative variations of the prefactors are observed[29,53]. Therefore, we base our simulations on the generic, bead-spring model by Kremer and Grest[54]. It has successfully reproduced the tribological behavior of adsorbed[55] and end-tethered[20] hydrocarbon films. Figure 1 shows our simulation-setup. The two surfaces are both curved and bear close to 4,000 polymers. For our default system, each polymer contains $N = 30$ repeat units, while some selected runs were repeated with a chain length of $N = 100$ beads. The polymers are tethered with one end to one surface with a density of approximately 2.5x the critical grafting density for brush formation. For most simulations 250,000 solvent atoms (dimers) are added, which makes the brushes slightly undersaturated. These simulations thus mimic a system where the solvent is in equilibrium with the vapor-phase and condenses into the brush[56] (i.e., our system would be comparable to experiments performed at a relative humidity of 90%[57]). In some selected runs, we studied the effect of (i) increasing the number of solvent atoms to full saturation or (ii) a complete immersion in solvent. In the latter we replaced the explicit solvent with a

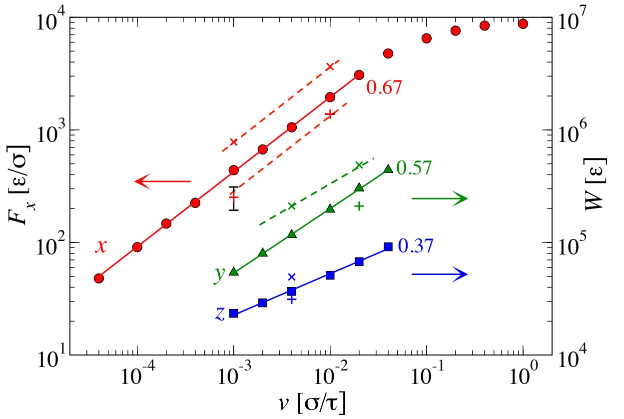

Fig. 2 Friction force F_x (red circles) during lateral motion in the x-direction and dissipated energy W for transverse motion in y (green triangles) and normal motion in z (blue squares) as a function of relative velocity v. The crosses (plus symbols) represent simulations in which the solvent viscosity is increased (decreased) by a factor of four. The solid lines are powerlaw fits to the color-matching data and the dashed lines are guides to the eye.

dissipative particle dynamics (DPD) thermostat, which correctly reproduces the hydrodynamics of the solvent[58]. In all simulations the interaction parameters were chosen such that the polymers are in good solvent conditions. More details on the setup can be found in the ESI†.

In the representation of our results, we use the reduced Lennard Jones units of the Kremer-Grest model. They translate to[54]: time $\tau = 3$ ps, length $\sigma = 0.5$ nm, energy $\varepsilon = 30$ meV and pressure P, $\varepsilon\sigma^{-3} = 40$ MPa. Our simulations are conducted in four modes: (a) motion along the symmetry or x-direction, mimicking sliding dynamics in an ideally conformal contact, (b) sliding along the y-direction, which probes lateral, off-center asperity collision, (c) mutual brush compression and decompression through normal motion in z, and (d) no motion at all. In modes (a)-(c) we simulate the motion at constant separation rather than constant load, to reproduce large stress fluctuations. In mode (d), we measure thermal force autocorrelation functions to gain insight in dissipation mechanisms close to equilibrium.

Results and Discussion

When sliding in x-direction, we probe similar dissipation mechanisms as in the parallel-plate geometry, where combing and subsequent solvent flow causes energy dissipation. Consequently, we find a sublinear $F \propto v^{\kappa}$ dependence similar to that identified previously[26] (see Fig. 2). Our exponent of $\kappa = 0.67$ is close to the estimate of $\kappa \approx 0.69$ for dry brush friction. However, upon sliding polymer-bearing surfaces at different velocities a velocity-dependent pressure-gradient in y is induced, which slightly increases our contact area. The latter causes our normal load to increase with increasing velocity more than expected solely due to shear-thinning of the system. By normalizing our friction force by the normal load we eliminate this effect to a linear approximation and consequently we find an exponent of $\kappa = 0.57$ in agreement with literature-values derived for semi-dilute brushes[26,59]. Test-runs show an effective exponent that is independent of the chain-length up to $N = 100$ beads and the amount of solvent absorbed into the brush. Moreover, by doubling the amount of solvent, the prefactor decreased with a factor 2-3, in agreement with experimental observations[56]. As shown in the ESI† (Fig.1), for small velocities our exponent is independent of the applied normal pressure between -30 and 400 MPa § ($\kappa = 0.67 \pm 0.02$).

In summary and in agreement with earlier observations[26], we find that for parallel sliding the scaling is independent of the normal load, brush characteristics and amount of absorbed solvent. The exponent for our curved surfaces is almost identical to exponents obtained for a parallel plate geometry. Therefore we conclude that for sliding at constant distance the shear-thinnning exponent is also independent of the capillary and the exact geometry for these and larger effective radii. The latter is consistent with the fact that the same scaling was observed in SFA experiments using a crossed-cylinder geometry[28] and MD simulations using a parallel plate geometry[26].

If the direction of sliding is changed to y, we no longer move parallel to a symmetry axis. The brushes are deformed viscoelastically, which includes partial squeeze-out of the solvent and its re–absorption. As a consequence, various additional features arise in the force traces during the periodic collision of two asperities, which is shown in Fig. 3a: (i) capillary breakup and formation near $y/L = 0.1$ (where L is the length of our simulation cell), (ii) a peak around $y/L = 0.5$, and (iii) a shoulder around $y/L = 0.8$. The instantaneous forces can be decomposed into dissipative and non-dissipative forces. The latter must have zero mean (averaged over one period) and be antisymmetric about the symmetry points ($y/L = 0$ and $y/L = 0.5$). The remaining contribution is symmetric and dissipative. Its average value corresponds to the mean kinetic friction $F_k = W/L$ with $W = \int_0^L F_y(y)dy$.

(i) Capillary dynamics is a thermally activated processes. This is why the positions of break-up and formation change logarithmically with v near $y/L = 0.1$. Locally, a friction force logarithmic in v would arise at small v, which would only cross over to linear response at extremely small velocities[60].

(ii) The first peak near $y/L = 0.5$ is symmetric and there-

---

§ For the conversion to real units we used the approximation that the normal force arises due to the deformation of the central 16 σ of the contact

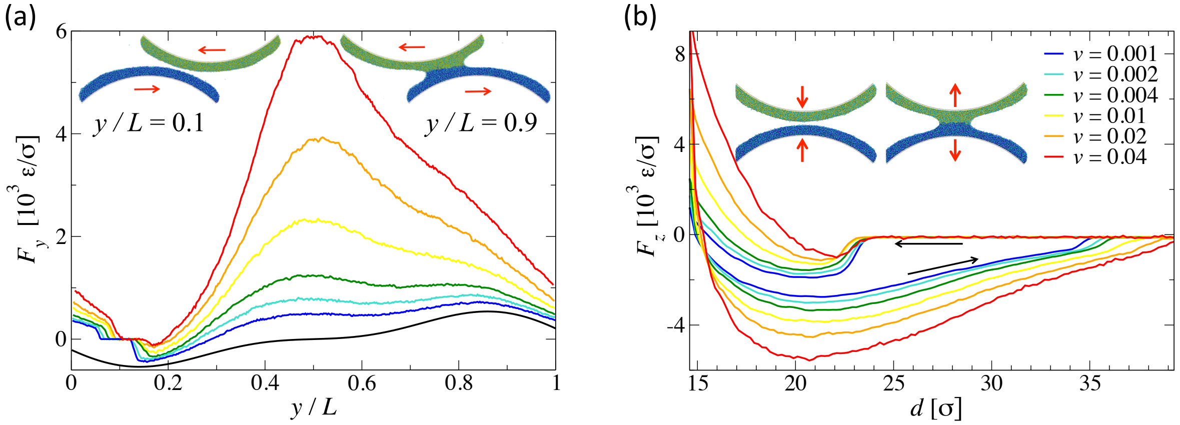

Fig. 3 (a) Force trace F_y of an asperity collision during transverse motion in y monitored over one period L (L is the length of our simulation cell) at different velocities v. The black line represents the equilibrium forces. (b) Force trace F_z during contact formation and break up under normal motion in z, where d denotes the distance between the solid surfaces. In the graphs, snapshots are inserted, which show the configuration at symmetry related points.

fore purely dissipative (see ESI† Fig. 2). At this point mainly shape hysteresis and steady state interdigitation control the dissipation, which we conclude from the overlap integral and analysis of the snapshots taken from the simulations. The height of the peak scales with $v^{0.69}$, i.e. similar to the scaling found in $F_x(y=L/2)$ when moving in x direction.

(iii) The shoulder in $\Delta F(v)$ in Fig. 3a turns into a (roughly symmetric) peak at $y/L \approx 0.78$ after subtracting the peak at $y/L = 0.5$ as well as the equilibrium force (see ESI† Fig. 2). The height of the second peak scales with $v^{0.67}$. As the second peak is not located at a symmetry point, both dissipative and non-dissipative forces contribute to it. This peak, therefore, must be caused by transient forces as earlier modeled for interdigitating soft-matter systems[61,62].

It is difficult to say what the relative contribution of each dissipation mechanism is to the mean friction force when moving parallel to y, since the relative contribution strongly changes in space and time. All mechanisms are intertwined (e.g. interdigitation affects both the capillary and shape hysteresis and vice versa), which again strongly depends on the velocity. This might explain why the mean kinetic friction also shows a power-law scaling just as individual dissipation mechanisms, interdigitation and shape hysteresis, do. The total integral scales with $v^{0.57}$ (see Fig.2). This exponent is the same as obtained for dissipation between fully solvated brushes in parallel plate geometries[26]. However, it is also close to the $\kappa = 0.54$ identified in simulation of off-center collisions between star polymers[43]. In the latter, the dissipation was related to *symmetry-breaking of the monomer density distribution*, a.k.a. shape hysteresis (interdigitation was found to be negligible). Thus, in the end it may be difficult to discriminate experimentally between the relative contributions of combing and viscoelasticity or alternative dissipation mechanisms.

When we increase the number of solvent atoms to full saturation, the second peak in the force trace becomes less pronounced and the effective exponent slightly increases. On the other hand, upon increasing the chain-length to $N = 100$ beads, the second peak becomes more pronounced and the extracted effective exponent slightly decreases. However, when we use the DPD thermostat to mimic complete immersion in solvent, the force trace significantly changes. There is no capillary breakup and the second peak strongly decreases (see ESI† Fig. 3) while our exponent increases to $\kappa = 0.65 \pm 0.06$. From the latter we can conclude that a capillary due to the surface tension of the solvent strongly enhances the transient effects resulting in a different effective scaling. Thus, in contrast to parallel sliding, changing the simulation parameters now changes the mix of dissipation mechanisms and thus alters the effective exponents.

When changing the motion to the direction perpendicular to the interface, we also observe transient forces amplifying shape and capillary hysteresis, see Fig. 3b, as previously for the y-direction. The total integral over the force now scales with a smaller exponent, namely with $v^{0.37}$ (see Fig. 2). For this head-on collision there will be a different relative contribution of the different dissipation mechanisms compared to an off-center collision. Consequently the exponent alters. However, having different responses in transverse and normal direction is to be expected even when there is a single dissipation mechanism (since the walls break the symmetry). Anisotropy in the pre-factors already occurs for simple liquids in linear response[63,64]. Thus, for more complex, shear-thinning liquids higher-order corrections can also be different and lead to different powerlaws outside linear response. This is yet another example for not having a stringent correlation between friction and adhesion[50].

In theoretical treatments of brush friction, the sublinear increase of F with v is believed to occur due to changes of polymer configurations, e.g., tilting of the brushes and reduction of overlap in response to shear. Locally, Stokes friction between polymer blobs, proportional to the solvent viscosity η, is assumed. However, in experiments it is regularly observed that the solvent viscosity is of minor importance[65] and that the friction force is strongly dependent on the amount of solvent absorbed into the brush[56,65]. To study this in more detail, we varied the solvent viscosity by multiplying the mass of solvent atoms with mass scaling factors of $s_m = 16$ and $s_m = 1/16$ while keeping all other parameters unchanged. In linear response, the frequency of a homogeneous mode, i.e., a mode involving an equal amount of solvent and polymer atoms, is proportional to $1/\sqrt{\rho_\mathrm{p} + s_m \rho_\mathrm{s}}$ (with ρ_p and ρ_s the default mass densities of polymer and solvent, resp.). For our system of interest, $\rho_\mathrm{p} = \rho_\mathrm{s}$ so that the frequencies of homogeneous modes rescale with $r = \sqrt{2/(1+16)} \approx 1/2.92$ for $s_m = 16$ and $r = \sqrt{2/(1+1/16)} \approx 1.37$ for $s_m = 1/16$. Thus, for our default system in linear response, one would expect an increase of the damping γ by a factor of 2.92 rather than 4 for the solvent isotope of $s_m = 16$.

Fig. 2 reveals that the solvent viscosity affects the dissipation strongest for lateral motion[¶], for which $\kappa = 0.67$ is largest and thus closest to linear response. Yet, the increase remains less than predicted, i.e., for $s_m = 16$, friction increases only by a factor of 2 rather than 2.92. The effect of the solvent viscosity on friction is smallest for normal motion ($\kappa = 0.37$, $\mathcal{O}(30\%)$). Our interpretation of this observation is that the local friction cannot be Stokes like. Instead local dynamics resembling instabilities (i.e., sudden, shear-induced changes from one configuration to the next stable or metastable configuration) determine the dissipated energy, irrespective of the precise duration of the jump (which does depend on η). When the dissipation is caused by instabilities, the damping affects the friction with the same exponent as the velocity[66–68], except for linear response at extremely small velocities. On a logarithmic scale, our data show a close resemblance to $F \propto (\gamma v)^\kappa$, which implies that polymer brush friction might be dominated by athermal second-order instabilities[69] and that, in agreement with experimental observations[65] the damping is determined by homogeneous modes instead of the solvent viscosity.

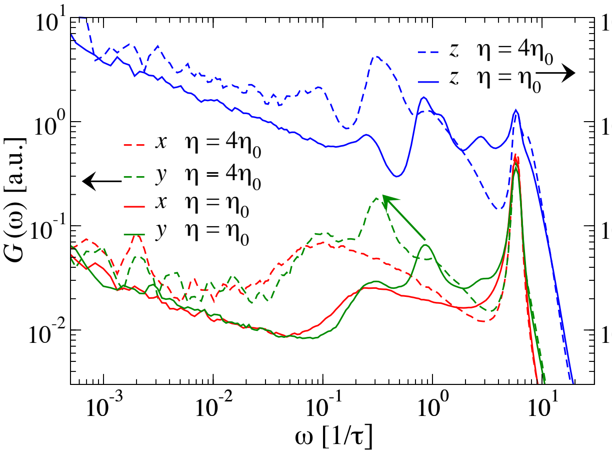

Fig. 4 Fourier transform $G(\omega)$ of the force autocorrelation function as a function of frequency ω. Different colors denote different directions, i.e., x (red), y (green), and z (blue). Straight lines refer to the default system, while dashed lines represent solvents with a viscosity η increased by a factor of four.

To elucidate the dissipation mechanism close to equilibrium we determine the force autocorrelation function, $G_{\alpha\alpha}(t) = \langle F_\alpha(t) F_\alpha(0) \rangle$. Here $F_\alpha(t)$ is the force on one surface at time t. We evaluate $G_{\alpha\alpha}(t)$ for each Cartesian coordinate α while keeping x, $y = L/2$, and z fixed. The Fourier transform of $G_{\alpha\alpha}(t)$ is related to the linear-response, frequency-dependent damping $\gamma(\omega)$ through the fluctuation-dissipation theorem via $\gamma(\omega) = \mathrm{Re}(G(\omega))/2k_BT$[70]. Fig. 4 shows $G(\omega)$ at a separation at which the load is slightly positive. Features do not change in a qualitative fashion between -30 and 400 MPa, except for the scaling at very small frequencies. High frequencies tend to reflect local vibrational dynamics, while low frequencies are long wavelength or relaxational dynamics. The high-frequency end of the spectra ($\omega > 5$) represent the quasi harmonic motion of the wall atoms. They remain unchanged when the solvent viscosity is increased. For frequencies $\omega < 5$, the spectra shift roughly with the predicted factor of 2.9 for high solvent viscosity, which means that the underlying dynamics consist of a concerted solvent-polymer motion. Upon doubling the amount of solvent in the brushes, the features in the spectra hardly change ($< 40\%$, see ESI† Fig. 4), which is most probably due to the change in brush height. This means that the friction reduction with increased solvent quantity, which is observed in the non-equilibrium simulations in x, must be a non-linear effect.

Since it takes roughly $T_\mathrm{wi} = 5\tau$ for information to travel from one wall to the interface and back[‖], features in the spectra reflecting interfacial properties must live at frequencies distinctly less than $\omega_\mathrm{wi} = 2/T_\mathrm{wi} = \mathcal{O}(0.4)$. The damping of

---

[¶] Note that for motion in x the viscosity does not affect the shear thinning exponent within the error bars, while for motion in y the effective exponent decreases to 0.51

[‖] The response time was found by measuring the time for a delta-pulse to travel from one surface to the opposing one.

the default system ($s_m = 1$) shows a peak near $\omega = 0.8$ for $\alpha = y,z$ (but not for $\alpha = x$). Because these peaks are too high in frequency to be sensitive to the interface, they can only be related to internal brush dynamics normal to the surface. In fact, averaged over the surface $\langle (n_y/n_z) \rangle = 0.3$ (with n the (local) unit vector), which roughly coincides with the ratio of $G_{yy}(\omega = 0.8) \approx 0.07$ and $G_{zz}(\omega = 0.8) \approx 0.2$. Thus, both peaks represent the same internal brush dynamics normal to the surface. Due to the curvature of our ridge, x has no component that is locally normal to the surface, and therefore there is no peak at this frequency. The peak in the damping in z at $\omega = 0.25$ represents the dissipation due to the capillary, which disappears when we apply a local brush non-overlapping constraint, which eliminates both brush overlap and the capillary due to the surface tension of the liquid. At very small frequencies, the default system shows $G(\omega) \propto \omega^{-\mu}$ with $\mu \approx 0.4$, implying a complex visco-elastic response controlled by many relaxation processes. In the x-direction, μ only slightly increases with the compression (see ESI† Fig. 5), consistent with recent AFM experiments studying the thermal response of interdigitated brushes[71]. For the x-direction the relaxation processes at small frequencies can only be due to interdigitation. In fact, $G_{xx}(\omega)$ no longer increases with decreasing ω for $\omega < 0.1$ ($\mu = 0$) when we apply the local brush non-overlapping constraint, while the spectral response for $\omega > 0.1$ remains unaltered. In the (y,z)-direction, our constraint does not strongly affect the scaling at small frequencies. However, μ increases with increasing compression (for z a lot stronger than for y). A similar effect was observed in experiments of the thermal response of a single brush with no interdigitation[72]. Therefore, we contribute the damping in z at small frequencies to the relaxation of global visco-elastic modes, while for y it is probably a combination of both interdigitation and global shape modes.

At the lowest frequencies ($\omega < 10^{-3}$ in Fig. 4) the frequency-dependent damping is almost independent of the solvent viscosity. For frequencies smaller than the slowest relaxation time in the system μ should go to zero. We cannot measure at which frequencies the damping levels off and consequently we cannot extract the effect of the solvent viscosity on the integrated damping for $\omega = 0$. Nevertheless, there is a range of frequencies for which the damping is independent of the solvent viscosity.

Although we mimicked roughness by employing curved surfaces, our system remains quite idealized. Therefore, a relevant question is: how do our results relate to realistic (experimental) systems? Our longest polymer-chains had a length $\sim$ 50nm, while polymers used in experiments are often longer. For parallel sliding, this will most likely not be a major issue, since we found no effect of the chain-length on the shear-thinning exponent. However, for asperity collisions, the chain length affects the relative importance of transient forces and thus the effective exponent. Additionally, real brushes will not have a single chain-length, but a chain-length distribution. For parallel sliding, this will, again, not affect the shear-thinning exponent. Yet, for sliding on rough surfaces, the effect of the chain-length is non-linear and thus a chain-length distribution will result in a different exponent compared to a single chain-length. In fact, it was recently shown for normal motion (head-on collisions) than polydispersity can qualitatively alter the dynamic response[73]. Moreover, the solvent used in experiments will not be as pure as ours. Real solvents will be 'contaminated' with other liquids and free-floating polymers. For parallel sliding the shear-thinning exponent was found to be independent of the amount/type of solvent. Nevertheless, for asperity collisions, the effective scaling strongly depends on the amount of solvent and on the surface tension and viscosity of the solvent. Therefore, also solvent-impurities in realistic systems will affect the rate-dependent friction-force for rough surfaces. On top of all this, in the present study we collided two asperities with a single curvature ($R = 50$nm). Real rough surfaces will have a non-uniform roughness distribution[74] and thus many different asperities of different shapes and sizes. Since the radius of curvature affects the scaling (for $R \rightarrow \infty$ we should obtain parallel sliding), the effective exponent for real rough surfaces will be different from ours.

Whether or not surface roughness will play a role in polymer brush friction depends on the dimensions of the system. It is intuitively plausible that there will be asperity collisions when the surface roughness amplitude is comparable or larger than the brush height. On the other hand, when the surface roughness amplitude is a lot smaller than the brush height, the brush interface will only show thermal roughness[75,76] that is uncorrelated with the surface roughness. Similar as described for simple liquids[77], there will be a healing length for polymer brushes. When the energetic cost due to surface tension of a curved interface is a lot higher than the energy penalty of an elastic deformation of the brush, the roughness of the interface will be thermally driven[75] and uncorrelated with the roughness of the surface. For a typical experimental setup of a polymer brush with a height > 100nm grafted onto a silicon surface with an average roughness amplitude of ± 1nm, the interfacial thermal roughness will be uncorrelated with the roughness of the surface. However, surfaces used in industry typically have a larger roughness amplitude[74] and so for industrial applications our results might become relevant. Moreover, it was shown in recent experiments that polymer brushes can only partly overcome the roughness of joint cartilage[78].

Our simulation show that the force maximum during an asperity collision (Fig. 3a) is not much higher than the steady-state friction force at the same velocity ($\sim 70\%$, see Fig. 2). Keeping in mind that the real contact area of rough surfaces in contact is only a small fraction of the apparent contact area[79] ($\sim 10^{-4}$), one can see that a small brushheight means a low friction force. Nevertheless, the brush should be high enough to prevent solid asperity collisions. thus, the optimal height will depend on the exact roughness distribution.

Interestingly, thermal fluctuations at the interface of the polymer brush will result in interfacial waves with a characteristic wavelength[75,76]. Thus, surface roughness can, depending on the exact roughness distribution, have a similar effect. Preliminary results show that, under specific circumstances, these interfacial waves can cause mono-dispersed asperity collisions after all, which will be subject of future research.

Conclusions

In summary, we have shown that the friction force for polymer brushes on rough surfaces can be qualitatively different from the friction for flat surfaces, resulting in different effective viscosities and shear-thinning exponents. We moved two parallel cylinders, decorated with end-anchored polymers, in the lateral, transverse and normal direction. For motion in the lateral direction, the distance between the walls remained constant during sliding and thus we studied a system comparable to idealized geometries. As expected, we observed that the dissipation is dominated by steady-state interdigitation. Moreover, we found a shear-thinning exponent that is independent of the normal load, brush characteristics, geometry, solvent viscosity or the amount of solvent, in agreement with earlier observations[26] for conformal contacts. Only the prefactors are affected by these parameters. Upon moving in the transverse direction, we mimicked the sliding of rough surfaces. We find that for asperity collisions transient interdigitation and capillary- and shape-hysteresis can contribute to the friction as much as steady-state interdigitation or even more. The exponents describing the rate dependence of the dissipation outside linear response now depend on the mix of different dissipation mechanisms. Consequently, now both the prefactor and the exponents depend on the normal load, brush characteristics, geometry and the amount/type of solvent. For normal motion the mix of dissipation-mechanisms was again different from transverse motion, resulting in a different exponent and so we reconfirm that there is no direct relation between friction and adhesion. The qualitative difference in the friction for rough and flat surfaces was also observed in the linear response regime. Finally, we found that the effect of the solvent viscosity on the prefactor in the friction force is sublinear, implying a deviation from Stokes-like dynamics in the polymer brush.

Ackowledgement

We thank the Jülich Supercomputing Centre for computing time.

References

1 F. P. Bowden and D. Tabor, *The Friction and Lubrication of Solids*, Oxford University Press Inc., New York, 2001.
2 T. Mang and W. Dresel, *Lubricants and Lubrication*, Wiley-VCH, Weinheim, 2007.
3 S. Lee and N. D. Spencer, *Science*, 2008, **319**, 575.
4 S. J. O'Shea, M. E. Welland and T. Rayment, *Langmuir*, 1993, **9**, 1826.
5 J. Klein, E. Kumacheva, D. Mahalu, D. Perahia and L. J. Fetters, *Nature*, 1994, **370**, 634.
6 L. Bureau and L. Léger, *Langmuir*, 2004, **20**, 4523.
7 S. Lee and N. D. Spencer, *Tribol. Int.*, 2005, **38**, 922.
8 J. P. Gong, *Soft Matter*, 2006, **2**, 544.
9 B. Zappone, M. Ruths, G. W. Greene, G. D. Jay and J. N. Israelachvili, *Biophys. J.*, 2007, **92**, 1693.
10 X. Sui, S. Zapotoczny, E. M. Benetti, P. Schön and G. J. Vancso, *J. Mater. Chem.*, 2010, **20**, 4981.
11 A. Li, E. M. Benetti, D. Tranchida, J. N. Clasohm, H. Schönherr and N. D. Spencer, *Macromolecules*, 2011, **44**, 5344.
12 T. Moro, Y. Takatori, K. Ishihara, T. Konno, Y. Takigawa, T. Matsushita, U.-I. Chung, K. Nakamura and H. Kawaguchi, *Nature Mater.*, 2004, **3**, 829.
13 J. F. Stanislav, *Rheol. Acta*, 1982, **565**, 564.
14 M. A. C. Stuart, W. T. S. Huck, J. Genzer, M. Müller, C. Ober, M. Stamm, G. B. Sukhorukov, I. Szleifer, V. V. Tsukruk, M. Urban, F. Winnik, S. Zauscher, I. Luzinov and S. Minko, *Nature Mater.*, 2010, **9**, 101.
15 S. Alexander, *J. Phys.-Paris*, 1977, **38**, 983.
16 P. G. de Gennes, *Macromolecules*, 1980, **13**, 1069.
17 J. Klein, *Annu. Rev. Mater. Sci.*, 1996, **26**, 581.
18 L. Léger, E. Raphaël and H. Hervet, *Advances in Polymer Science*, 1999, **138**, 185.
19 G. S. Grest, *Phys. Rev. Lett.*, 1996, **76**, 4979.
20 K. Binder, T. Kreer and A. Milchev, *Soft Matter*, 2011, **7**, 7159.
21 T. Kreer, M. H. Müser, K. Binder and J. Klein, *Langmuir*, 2001, **17**, 7804.
22 W. K. den Otter and S. A. Shkulipa, *Biophys. J.*, 2007, **93**, 423.
23 T. A. Witten, L. Leibner and P. A. Pincus, *Macromolecules*, 1990, **23**, 824.
24 Y. B. Zhulina, V. A. Pryamitsyn and O. V. Borisov, *Polym. Sci. USSR*, 1989, **31**, 205.
25 J.-F. Joanny, *Langmuir*, 1992, **8**, 989.
26 A. Galuschko, L. Spirin, T. Kreer, A. Johner, C. Pastorino, J. Wittmer and J. Baschnagel, *Langmuir*, 2010, **26**, 6418.
27 J.-M. Y. Carrillo, D. Russano and A. V. Dobrynin, *Langmuir*, 2011, **27**, 14599.
28 P. A. Schorr, T. C. B. Kwan, S. M. Kilbey, E. S. G. Shaqfeh and M. Tirrell, *Macromolecules*, 2003, **36**, 389.
29 Y. Ou, J. B. Sokoloff and M. J. Stevens, *Phys. Rev. E*, 2012, **85**, 011801.
30 L. Spirin and T. Kreer, *ACS Macro Lett.*, 2013, **2**, 63.
31 F. Goujon, A. Ghoufi, P. Malfreyt and D. J. Tildesley, *Soft Matter*, 2013, **9**, 2966.
32 J. B. Sokoloff, *J. Chem. Phys.*, 2008, **129**, 014901.
33 U. Raviv, S. Giasson, N. Kampf, J.-F. Gohy, R. Jerome and J. Klein, *Nature*, 2003, **425**, 163.
34 C. Drummond, *Phys. Rev. Lett.*, 2012, **109**, 154302.
35 C. Xu, R. L. Jones and J. D. Batteas, *Scanning*, 2008, **30**, 106.
36 B. W. Ewers and J. D. Batteas, *J. Phys. Chem C*, 2012, **116**, 25165.
37 D. A. Hook, S. J. Timpe, M. T. Dugger and J. Krim, *J. Appl. Phys.*, 2008, **104**, 034303.
38 F. Goujon, P. Malfreyt and D. J. Tildesley, *Soft Matter*, 2010, **6**, 3472.
39 E. Svetushkina, N. Puetskiy, L. Ionov, M. Stamm and A. Synytska, *Soft Matter*, 2011, **7**, 5691.

40 C. Drummond, J. Rodríguez-Hernández, S. Lecommandoux and P. Richetti, *J. Chem. Phys.*, 2007, **126**, 184906.

41 D. Tabor, *Rubber Chem. Technol.*, 1958, **33**, 142.

42 B. N. J. Persson, *J. Phys. Chem.*, 2001, **115**, 3840.

43 S. P. Singh, R. G. Winkler and G. Gompper, *Phys. Rev. Lett.*, 2011, **107**, 158301.

44 W. J. Briels, *Soft Matter*, 2009, **5**, 4401.

45 P. A. Nommensen, M. H. G. Duits, D. van den Ende and J. Mellema, *Phys. Rev. E*, 1999, **59**, 3147.

46 J. Klein, Y. Kamiyama, H. Yoshizawa, J. N. Israelachvili, G. H. Fredrickson, P. Pincus and L. J. Fetters, *Macromolecules*, 1993, **26**, 5552.

47 E. Riedo, F. Lévy and H. Brune, *Phys. Rev. Lett.*, 2002, **88**, 185505.

48 S. Derler and L. C. Gerhardt, *Tribol. Lett.*, 2012, **45**, 1.

49 B. N. J. Persson, A. Kovalev and S. N. Gorb, *Tribol. Lett.*, 2013, **50**, 17.

50 H. Yoshizawa, Y.-L. Chen and J. Israelachvili, *J. Phys. Chem.*, 1993, **97**, 4128.

51 A. Dhinojwala, L. Cai and S. Granick, *Langmuir*, 1996, **12**, 4537.

52 J. Ringlein and M. O. Robbins, *Am. J. Phys.*, 2004, **72**, 884.

53 M. K. Vyas, K. Schneider, B. Nandan and M. Stamm, *Soft Matter*, 2008, **4**, 1024.

54 K. Kremer and G. S. Grest, *J. Chem. Phys.*, 1990, **92**, 5057.

55 G. He, M. H. Müser and M. O. Robbins, *Science*, 1999, **284**, 1650.

56 M. Kobayashi, Y. Terayama, N. Hosaka, M. Kaido, A. Suzuki, N. Yamada, N. Torikai, K. Ishihara and A. Takahara, *Soft Matter*, 2007, **3**, 740.

57 M. Biesalski, D. Johannsmann and J. Rühe, *Macromol. Symp.*, 1999, **145**, 113.

58 C. Pastorino, T. Kreer, M. Müller and K. Binder, *Phys. Rev. E*, 2007, **76**, 026706.

59 L. Spirin, A. Galuschko, T. Kreer, A. Johner, J. Baschnagel and K. Binder, *Eur. Phys. J. E*, 2010, **33**, 307.

60 M. H. Müser, *Phys. Rev. B*, 2011, **84**, 125419.

61 A. van den Noort, W. K. den Otter and W. J. Briels, *EPL*, 2007, **80**, 28003.

62 W. J. Briels, D. Vlassopoulos, K. Kang and J. K. G. Dhont, *J. Chem. Phys.*, 2011, **134**, 124901.

63 H. Brenner, *Chem. Eng. Sc.*, 1961, **16**, 242.

64 M. Schindler, *Chem. Phys.*, 2010, **375**, 327.

65 M. T. Müller, X. Yan, S. Lee, S. S. Perry and N. D. Spencer, *Macromolecules*, 2005, **38**, 5706.

66 E. Raphaël and P. G. de Gennes, *J. Chem. Phys.*, 1989, **90**, 7577.

67 J.-F. Joanny and M. O. Robbins, *J. Chem. Phys.*, 1990, **92**, 3206.

68 Y. Sang, M. Dubé and M. Grant, *Phys. Rev. Lett.*, 2001, **87**, 174301.

69 M. H. Müser, *Phys. Rev. Lett.*, 2002, **89**, 224301.

70 R. Kubo, *Rep. Prog. Phys.*, 1966, **29**, 255.

71 O. von Sicard, A. M. Gigler, T. Drobek and R. W. Stark, *Langmuir*, 2009, **25**, 2924.

72 F. Benmouna and D. Johannsmann, *J. Phys.: Condens. Matter*, 2003, **15**, 3003.

73 S. M. Balko, T. Kreer, P. J. Costanzo, T. E. Patten, A. Johner, T. L. Kuhle and C. M. Marques, *PLoS ONE*, 2013, **8**, e58392.

74 B. N. J. Persson, O. Albohr, U. Tartaglino, A. I. Volokitin and E. Tosatti, *J. Phys.: Condens. Matt.*, 2005, **17**, R1.

75 G. H. Fredrickson, A. Ajdari, L. Leibler and J.-P. Carton, *Macromolecules*, 1992, **25**, 2882.

76 G. Fytas, S. H. Anastasiadis, R. Seghrouchni, D. Vlassopoulos, J. Li, B. J. Factor, W. Theobald and C. Toprakcioglu, *Science*, 1996, **274**, 1698.

77 M. O. Robbins, D. Andelman and J.-F. Joanny, *Phys. Rev. A*, 1991, **43**, 4344.

78 N. Wang, A.-M. Trunfio-Sfarghiu, D. Portinha, S. Descartes, E. Fleury, Y. Berthier and J.-P. Rieu, *Colloids Surf. B*, 2013, **108**, 285.

79 M. H. Müser, M. Urbakh and M. O. Robbins, *Adv. Chem. Phys.*, 2003, **126**, 187.